

SPG Mitteilungen Communications de la SSP

Auszug - Extrait

Milestones in Physics (23)

Origin of the Elements Part II: from Fe to Pb and the Actinides

Friedrich-Karl Thielemann

Department of Physics, University of Basel and GSI Helmholtz Center for Heavy Ion Research, Darmstadt

This article has been downloaded from:
https://www.sps.ch/fileadmin/articles-pdf/2021/Mitteilungen_Milestones_23.pdf

© see https://www.sps.ch/bottom_menu/impressum/

Milestones in Physics (23)

Origin of the Elements Part II: from Fe to Pb and the Actinides

Friedrich-Karl Thielemann

Department of Physics, University of Basel and GSI Helmholtz Center for Heavy Ion Research, Darmstadt

Part I of this series concentrated on the understanding of element abundances (and their creation) in the Universe up to Fe, Ni, and Zn. With respect to stellar contributions it was restricted to the evolution of single stars and did not include binary systems. There exists an important contribution to Fe and elements in its vicinity from type Ia supernovae and to the production of the heaviest elements from neutron star mergers, both originating from binary systems. Therefore, this part II adds a discussion of element production up to Zn from binary stellar systems and presents the origin of all heavier elements in a joint review for both types of stellar (single and binary) systems.

Binary stellar systems and their explosive endpoints:

The majority of stars are born in binary and multiple stellar systems. The gravitational interaction among them can lead to mass exchange and mergers, affecting their final fate. This can take place (a) via mass overflow, when one of the binary members fills the so-called Roche Lobe and the attraction for mass elements of one binary towards the other binary member can supersede its own gravity (the Roche lobe is the critical equipotential surface of the joint system for which the individual equipotential surfaces of both binary members touch in one point). The other option (b) is that the emission of gravitational waves causes rotational energy loss and a reduction of the distance of the two members, resulting in an inspiral and a merger of both objects. (a) can be important when one of the members experiences tremendous radius changes by a factor of 100 or more, e.g. during the transition from an H-burning main sequence star to a red giant after the central H-core is exhausted. This leads to the expansion beyond the Roche lobe and therefore mass overflow. (b) involves often binary systems with both members being already in their final stage of stellar evolution, i.e. compact objects like white dwarfs (after a planetary nebular event), neutron stars (after a supernova explosion) or black holes (resulting from failed supernovae of very massive stars). Such systems are typically in thermodynamic conditions of a *cold (degenerate) Fermi gas* (electrons in white dwarfs, nucleons and electrons in neutron stars), where the pressure $P(\rho, T)$ depends only on the density and lost its temperature dependence. Mass transfer of unburned hydrogen from the outer layers of the companion (termed accretion) onto the surface of compact objects can lead to ignition and an energy release by nuclear reactions which enhances the exponentially temperature-dependent thermonuclear reaction rates, while initially the pressure (due to the still lacking temperature dependence) is not increasing. The latter could otherwise control and stabilize the situation via expansion of matter and pressure reduction. Such thermonuclear runaways, causing an exploding behavior once the degeneracy is lifted (i.e. the temperature dependence is reinstated), lead to explosive hydrogen burning, causing **nova events** on the surface of white dwarfs and **X-ray bursts** on the surface of neutron stars. If the accreting mass

overflow is larger, it causes a temperature increase already during the accretion, avoiding ignition under degenerate conditions and permitting e.g. subsequent quiescent H- and He-burning on the surface of an accreting white dwarf. This way the mass of the initially existing C/O white dwarf can grow towards the critical Chandrasekhar mass. When this limit is reached, contraction sets in, causing central degenerate ignition of C-burning. It is also possible that a thermonuclear runaway He-ignition sets in at the base of the He-zone before the accreting white dwarf reaches the Chandrasekhar mass, causing a shock wave propagating to the center where C is ignited explosively. Both cases lead to a complete explosive disruption of the white dwarf, known as **type Ia** (Chandrasekhar-mass or sub-Chandrasekhar) **supernova**. Both of these explosive ignitions are of the type (a). On the other hand, the gravitational inspiral (b) of binary white dwarfs can also lead to type Ia supernovae, and the inspiral of a binary neutron star system leads to neutron star mergers. We will not discuss here in detail novae and X-ray bursts, as their nucleosynthesis contribution to our known abundance pattern is close to negligible. Novae, due to high temperatures attained in H-burning, burn H in the accreted material not via the well-known CNO-cycle (see Fig. 5 in part I), but in the so-called hot CNO cycle. It is characterized by the fact that in the branching between the slow beta-decay of ^{13}N and a further proton capture to ^{14}O , the proton capture wins because of a highly enhanced reaction rate for such conditions. In a similar way hot CNO-type cycles for elements beyond Ne re-arrange nuclei up to Mg and Si. When including ejecta of such nova explosions, a few not highly abundant isotopes up to Mg and Si can be considered to have a non-negligible contribution from novae. In type I X-ray bursts, due to the explosive ignition of H- and subsequent He-burning reactions, matter from the hot CNO cycle can even be transferred to heavier nuclei up to ^{100}Sn . This is an important stellar explosion, observed in X-rays, but the explosion energy is likely not sufficient to eject matter out of the high gravitational binding of the neutron star. While some elements can be identified in the observed X-ray spectra, such events do very likely not contribute to our universal abundance pattern. For these reasons we will concentrate here on type Ia supernovae and neutron star, as well as neutron star – black hole mergers. A detailed discussion of novae and X-ray bursts can be found in JOSÉ (2016), the evolution of knowledge on the nuclear reactions involved from WIESCHER ET AL. (1986) over CYBURT ET AL. (2010) to MEISEL ET AL. (2020).

Type Ia supernovae:

Fig. 1 shows case (a) of a binary system containing an advanced star and a white dwarf (the “single degenerate” option), leading here to a Chandrasekhar-mass type Ia supernova event. The early understanding of type Ia supernovae goes back to HOYLE & FOWLER (1960). First *carbon-detonation* models of a Chandrasekhar-mass white dwarf were de-

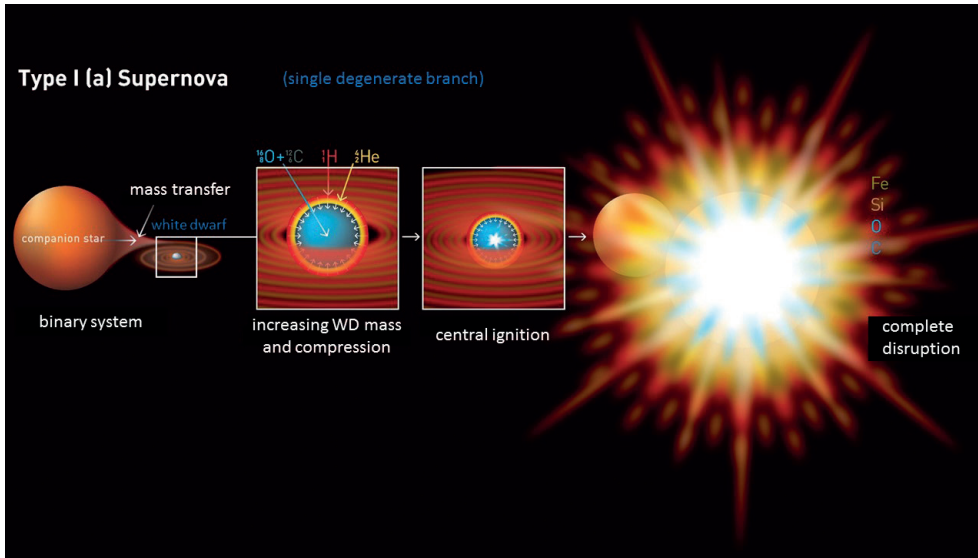


Fig. 1: Evolution of a binary system with one star in an advanced burning stage (a red giant that increased its radius by a factor of 100 or more after central H-burning, permitting under these conditions the mass transfer to the companion white dwarf). For sufficiently high accretion rates H (and subsequently He) burns quiescently, increasing the mass of the original C/O white dwarf towards the critical Chandrasekhar limit, causing compression and central C-ignition which ends in a complete explosive disruption of the object.

veloped by ARNETT (1969), ARNETT ET AL. (1971), and WOOSLEY ET AL. (1986). A detonation involves a burning front which propagates in excess of the sound speed for matter ahead of the front. This does not permit pre-expansion of the material and burns (if ignited with a strong artificial flame for high densities with $\rho > 10^7 \text{ g cm}^{-3}$, as experienced in the center of Chandrasekhar-mass white dwarfs) essentially the whole white dwarf to nuclei with the highest binding energies in the Fe-group, which did not fit observational spectra. IBEN & TUTUKOV (1984) and WEBBINK (1984) laid the theoretical groundwork for the so-called single and double degenerate (white dwarf merger) systems. First 1D *carbon-deflagration* models with subsonically propagating burning fronts were developed by NOMOTO (1982), NOMOTO ET AL. (1984) and WOOSLEY & WEAVER (1986). Here the burning front starts in the center only with the speed permitted by heat conduction (due to the mean free path of electrons) which is smaller than sound speed, resulting in explosions where in the outer layers unburned matter survives. MÜLLER & ARNETT (1986) and later KHOKLOV, MÜLLER & HÖFLICH (1993) started general combustion approaches, including so-called delayed detonations, where a transition from an initial deflagration to a detonation takes place. Presently, in addition to single-degenerate Chandrasekhar-mass systems, starting with a central or off-center carbon ignition, also single degenerate systems with He-ignition in accreted matter, before the Chandrasekhar mass is attained, are considered. Such sub-Chandrasekhar models are triggered by double detonations, where a detonation is ignited in outer layers at the bottom of the accreted He-zone, resulting also in an inward moving compression wave which causes finally a central ignition, but in a pre-expanded medium with a density $\rho < 10^7 \text{ g cm}^{-3}$, avoiding unwanted abundance features from central detonations in Chandrasekhar-mass white dwarfs. The major problem for all these approaches is that a fully self-consistent simulation, resulting in a thermonuclear ignition at high densities but initially low temperatures, is problematic in grid-based codes, because they are limited in their timesteps by the sound speed between grid points, causing excessive computing demands (ZINGALE ET AL. 2018). Instead in most cases

artificially ignited flames (and their distributions) have been utilized. This problem can be avoided in dynamical events like double degenerate mergers. Even (to a small fraction) white dwarf collisions can lead to type Ia supernovae (for a general review of all scenarios see HÖFLICH ET AL. 1998, HILLEBRANDT ET AL. 2013, PAKMOR ET AL. 2013, DAN ET AL. 2015, MAEDA & TERADA 2016, GARCIA-SENZ ET AL. 2016, JIANG ET AL. 2017, RÖPKE & SIM 2018, THIELEMANN ET AL. 2018, SHEN ET AL. 2018, LEUNG & NOMOTO 2018). At present the major aid is coming from observational features, disentangling the possible scenarios which lead to the full sample of observations (MAOZ ET AL. 2014, NOEBAUER ET AL. 2017, GOLDSTEIN & KASEN 2018, SEITENZAHL ET AL. 2019) in combination with galactic evolution tests.

Important aspects for understanding the combination of contributing sce-

narios are coming from their nucleosynthesis contributions, e.g. in addition to the dominant Fe production the behavior of Mn (from ^{55}Co -decay) and Zn production in galactic evolution (SEITENZAHL & TOWNSLEY 2017, HÖFLICH ET AL. 2017, LEUNG & NOMOTO 2018, MISHENINA ET AL. 2015, TSUJIMOTO & NISHIMURA 2018, LACH ET AL. 2019, PALLA 2021, GRONOW ET AL. 2021). When having a look at Fig. 2 of part I, one sees (i) the impact of the strong Fe-production (mainly from ^{56}Ni -decay) at metallicities of $[\text{Fe}/\text{H}] = -1$. The slow stellar evolution of stars turning into white dwarfs with originally low and intermediate masses $< 8 M_{\odot}$ delays this process, plus the evolution of the binary system to mass transfer or a merger. This can be seen in the $[\text{O}/\text{Fe}]$, $[\text{Mg}/\text{Fe}]$, $[\text{Si}/\text{Fe}]$, $[\text{S}/\text{Fe}]$, $[\text{Ca}/\text{Fe}]$, $[\text{Ti}/\text{Fe}]$ downturns at $[\text{Fe}/\text{H}] = -1$. On the other hand Mn is rising at this point, i.e. type Ia supernovae must be a strong contributor of Mn. This can be seen in Fig. 2, which shows an early (spherically symmetric) simulation of the carbon-deflagration model W7 by NOMOTO ET AL. (1984), THIELEMANN ET AL. (1986), and more recent 2 and 3D simulations (MAEDA ET AL. 2010, TRAVAGLIO ET AL. 2011, 2018). In Chandrasekhar-mass deflagration models ^{55}Co is produced in the inner regions of explosive Si-burning due to Y_{e} -values which result from electron capture on free protons and nuclei at high densities (with high electron Fermi energies). In the outer regions incomplete Si-burning and a Y_{e} due to the metallicity of the object (see Fig. 2 caption) leads to similar results. Sub-Chandrasekhar mass single-degenerate models do not experience the high density conditions in the central parts, but they find similar conditions as shown in Fig. 2 for the outer parts, due to a Y_{e} inherited from the metallicity of the objects. Thus, both types of scenarios (Chandrasekhar as well as sub-Chandrasekhar models) could therefore explain the rise of $[\text{Mn}/\text{Fe}]$ due to the onset of type Ia supernovae in galactic evolution for metallicities $[\text{Fe}/\text{H}] > -1$. Similar aspects are discussed in PALLA (2021) and GRONOW ET AL. (2021) also for V, Cr, and Ni.

Another feature which still needs to be explained is the behavior of $[\text{Zn}/\text{Fe}]$ (see also Fig. 2 of part I), which stays

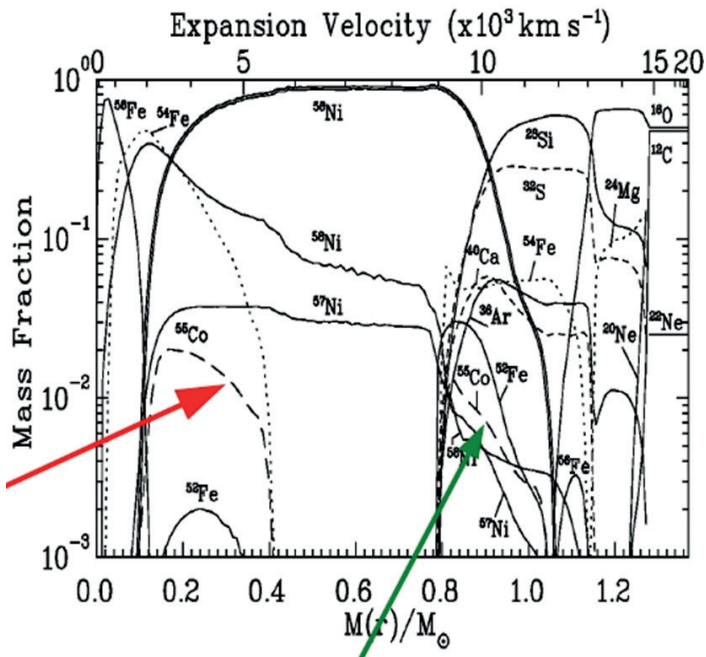
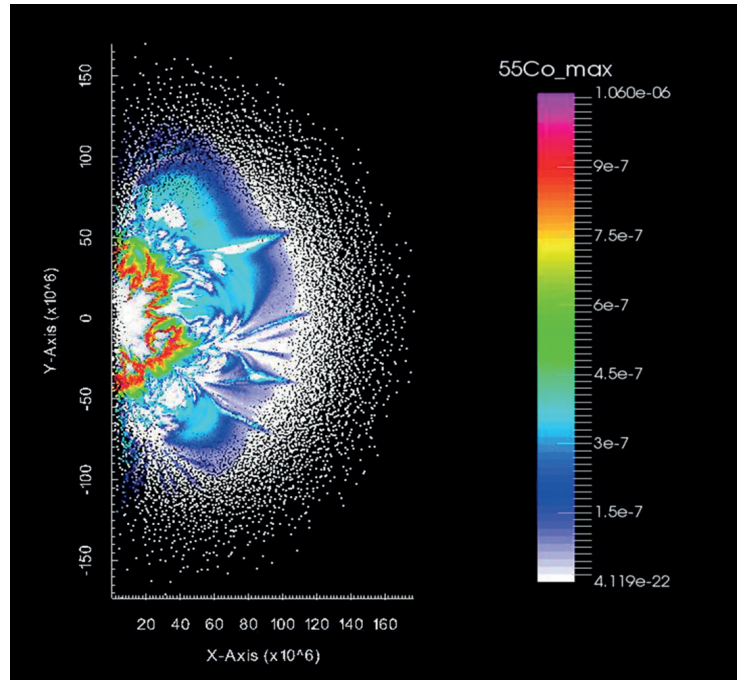


Fig. 2: The left panel shows the nucleosynthetic composition of the first W7 carbon-deflagration model after the explosion (NOMOTO ET AL. 1984, THIELEMAN ET AL. 1986). The bottom x-axis indicates the position in terms of radial mass zones from the center to the surface of the exploding white dwarf (close to a Chandrasekhar mass of $1.4 M_{\odot}$), the top x-axis shows the respective expansion speed of that matter after the explosion. The y-axis indicates the mass fractions of (a few) important species produced. One notices about $0.6 M_{\odot}$ of ^{56}Ni (decaying later to ^{56}Fe) and in the outer layers the results of incomplete (Si, O, Ne, and C-) burning, leaving even unburned fractions of C and O at the surface. An interesting aspect is that in the central regions stable ^{56}Fe and ^{54}Fe are produced directly, being more neutron-rich than ^{56}Ni , due to the high Fermi energies of electrons in degenerate matter and electron capture on protons and nuclei (turning a free or bound proton into a neutron). This effect is measured by Y_e (the total proton/nucleon ratio,

constant during galactic evolution across the $[\text{Fe}/\text{H}] = -1$ boundary dominated by core-collapse supernovae or type Ia supernovae, respectively. The Zn in core-collapse supernovae is made in high entropy explosive Si-burning, where matter is in an alpha-rich freeze-out processed beyond ^{56}Ni up to ^{60}Zn and ^{64}Ge (decaying to ^{64}Zn). Chandrasekhar-mass models seem not to be able to result in such conditions. The open question is whether specific conditions of He-detonations in sub-Chandrasekhar models might nevertheless be able to do this (LACH ET AL. 2020) or whether binary merger double-degenerate systems can do so. In order for $[\text{Zn}/\text{Fe}]$ to stay constant during galactic evolution across the $[\text{Fe}/\text{H}] = -1$ boundary, also a fraction of type Ia supernovae has to experience such conditions.

As can be seen from the discussion above, the dominant scenario for type Ia supernovae is not fully determined, yet, but observations indicate that apparently all of the mentioned scenarios can contribute. Nevertheless, a defining feature is that type Ia supernova models produce on average about $0.6 M_{\odot}$ of ^{56}Ni , decaying to ^{56}Fe in comparison to about $0.1 M_{\odot}$ from core-collapse supernovae (see part I). Therefore type Ia supernovae are a major or the dominant producer of Fe in galaxies (the higher frequency of core-collapse events makes up about a factor of 4 - 5). In addition, light curve observations of the whole class lead to an empirical relation between their maximum luminosity (related



with 0.5 for symmetric nuclei). This process is also responsible for producing ^{55}Co (decaying later to ^{55}Mn) in the inner layers between 0.1 and $0.4 M_{\odot}$ (red arrow) and responsible for the increase of $[\text{Mn}/\text{Fe}]$ in Fig. 2 of part I at $[\text{Fe}/\text{H}] = -1$. The green arrow points to a region where no electron capture occurred and Y_e is determined by the initial metallicity of the white dwarf or the accreted matter. In H-burning via the CNO-cycle all CNO nuclei are turned to ^{14}N (with the slowest proton-capture reaction) and in subsequent He-burning this is turned into ^{22}Ne via $^{14}\text{N}(\alpha, \gamma)^{18}\text{F}(\beta^+)^{18}\text{O}(\alpha, \gamma)^{22}\text{Ne}$, a nucleus which is with $N = Z + 2$ slightly neutron-rich. Thus, the fraction of ^{55}Co in the outer zones is dependent on pre-existing CNO, but the more central part is a unique feature of the single-degenerate Chandrasekhar-mass branch of type Ia supernovae. The right panel shows the results of a 2D simulation by TRAVAGLIO ET AL. (2018), where the same ^{55}Co enhancement can be seen, just in a more general, non-spherically symmetric, topology.

to the ^{56}Ni mass) and the luminosity decline as a function of time. This way they can act as standardizable candles to determine their intrinsic brightness and can therefore be utilized as distance indicators, which permitted to understand the accelerated expansion of the Universe (leading to Nobel Prizes for Perlmutter, Riess, and Schmidt in 2011 “for the discovery of the accelerating expansion of the Universe through observations of distant supernovae”, see part I).

The Formation of Heavy Elements:

While we have mentioned above nucleosynthesis aspects of binary stellar systems with mass exchange (novae, X-ray burst, type Ia supernovae), we have up to now not presented a detailed discussion of neutron star and neutron star - black hole mergers. Before doing so, we want to address in a more general way the basic mechanisms how heavy nuclei much beyond Fe, Ni, and Zn can be produced, before going into specific stellar environments. In part I we discussed the general density and temperature dependence of reaction rates. Capture reaction rates go linear with density. Neutron capture reaction rates have close to no temperature dependence, because the energy or velocity distribution of neutrons for a given plasma temperature cancels with the energy dependence of neutron capture cross sections for dominant s-wave neutrons. Charged-particle reaction rates show, however, an exponentially increasing temperature dependence due to Coulomb repulsion. This

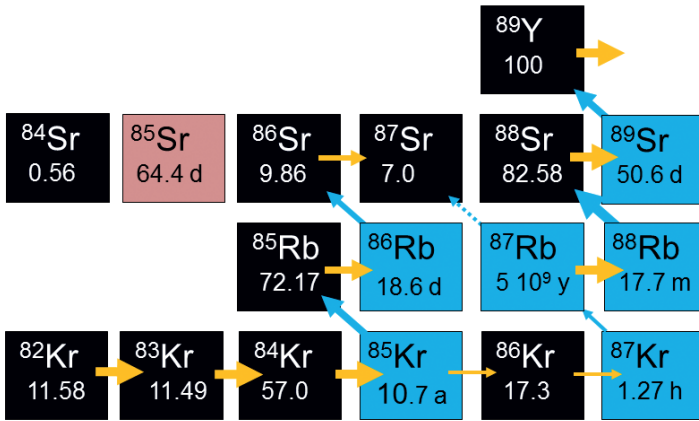


Fig. 3: left panel (courtesy of F. Käppeler), neutron captures connect isotopes with neutron number N and $N + 1$ of the same element with charge number Z until a β -unstable nucleus decays to the next isotopic chain with $Z + 1$. For very long-lived nuclei a further neutron capture can win against beta-decay and a branching in the s-process path occurs. A pure s-nucleus is ^{86}Sr , as nuclei which would be produced by the more neutron-rich r-process would end up via beta-decay in ^{86}Kr , blocking any r-process con-

tribution to ^{86}Sr . The right panel (courtesy of R. Reifarth) shows abundance results Y_A of s-process simulations for pure s-process nuclei from two exponential superpositions of neutron exposures τ_n , multiplied with the related neutron capture cross section σ_A . Horizontal lines with $\sigma_A Y_A = \text{const}$ show regions of a steady-flow equilibrium of neutron captures. The weak s-process branch up to $A = 90$ requires weaker neutron exposures.

is the main reason why stars undergo in subsequent burning stages (with increasing temperatures) fusion reactions of increasingly heavier nuclei. On the other hand, photodisintegrations are also exponentially temperature dependent. For typical densities in stellar evolution (due to the only linear density dependence of capture reactions, but highly exponential temperature dependence of photodisintegrations) photodisintegrations win against the inverse capture reaction if temperatures kT are in excess of the reaction Q -value divided by 30 ($Q/30$), as a rule of thumb. This will, with the increasing charge numbers of heavy nuclei, forbid charged-particle capture reactions much beyond the Fe-group, because the required temperatures for permitting charged-particle captures would lead to a dominance of the reverse photodisintegrations. Therefore, with few exceptions, like for high densities in X-ray burst in the accreted matter on top of neutron stars or in the νp -process of the innermost regions of core-collapse supernovae (see part I), the formation of heavy nuclei much beyond Fe is not possible via charged-particle reactions. Thus, the preferred way towards heavy nuclei is paved with neutron captures (as already outlined by BURBIDGE ET AL. 1957 and CAMERON 1957), with a close to vanishing temperature dependence of the related reaction rates. With the short lifetimes of neutrons, on the order of 10 min, it appears as if Nature experienced apparently only two major sets of conditions where such series of neutron captures can occur: (a) during stellar evolution where a continuous production of neutrons can take place via (α, n) -reactions, or (b) explosive events where due to these explosions suddenly high densities of neutron can be released on short timescales. (a) leads to the slow neutron capture (or s-) process, where due to the low neutron densities generally beta-decays win over neutron captures. (b) can produce highly neutron-rich isotopes far from stability before beta-decays take place, leading to the rapid neutron capture (or r-) process.

The **s-process** is related to late stellar burning phases after core H-burning, when stars have turned into red giants with a large radius increase. In the subsequent He-burning phase (α, n) -reactions can release neutrons. One simple option is $^{22}\text{Ne}(\alpha, n)^{25}\text{Mg}$. As was discussed in the caption of

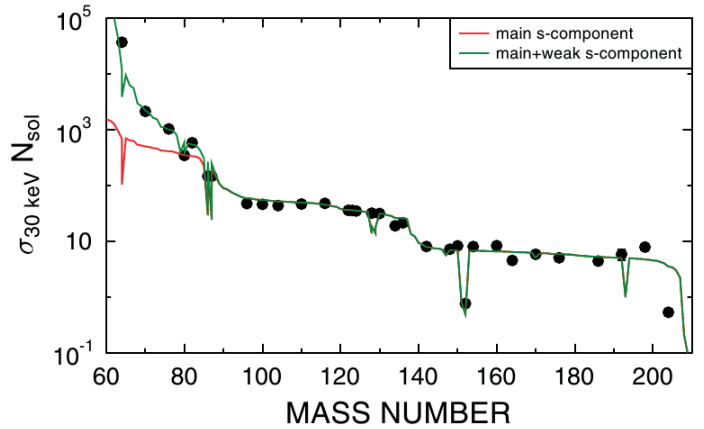


Fig. 2, ^{22}Ne is created in He-burning, acting on H-burning product ^{14}N . The neutrons from this source lead in central He-burning of massive stars to the so-called weak s-process with the formation of nuclei up to $A = 90$ (found by LAMB ET AL. 1977), via neutron captures and β -decays. A reaction path is shown in Fig. 3 (left panel), indicating neutron captures in horizontal steps within the isotopic chain of charge Z , and β -decays to nucleus $(Z + 1, N - 1)$ with the same mass number A . In most cases the beta-decays are much faster than neutron captures for these low neutron densities and the s-process passes through a path of stable nuclei, with a unique identification of nuclei for each mass number A . In the case of very long-lived nuclei (longer than the typical neutron-capture timescales in the s-process of months to years), permitting a further neutron capture, also branchings can be noticed (see ^{85}Kr in Fig. 3).

With a unique identification of mass number $A = Z + N$ with a specific nucleus (Z, N) in the s-process path (when beta-decays can be viewed as instantaneous), one can think of the s-process path as a chain of neutron captures, where the progress is only determined by the neutron exposure $\tau_n = \int n(t) dt$, which integrates the neutron density of the environment over time (first suggested by SEEGER ET AL. 1965). With neutron capture cross sections known for stable nuclei, the abundances can be predicted as a function of A , dependent on the neutron exposure τ_n . What is shown in the right panel of Fig. 3 is actually based on an exponential superposition of neutron exposures. In a steady flow of neutron captures the flow from nucleus $A - 1$ to nucleus A should be the same as the flow from A to $A + 1$, resulting in $\langle \sigma v \rangle_{A-1} Y_{A-1} = \langle \sigma v \rangle_A Y_A = \text{const}$. With the same neutron velocity distribution in a given environment this can also be written as $\sigma_A Y_A = \text{const}$. We see in Fig. 3 that this is essentially fulfilled for nuclei between the neutron shell closures at $N = 50, 82, \text{ and } 126$. The exceptions with multiple entries are branchings, like the ones in the left panel. For the shell closures $N = 50, 82, 126$ and for $A < 90$ (or $N < 50$), such an equilibrium is not attained because the too small capture cross sections do not permit a steady-flow equilibrium for the small neutron densities experienced.

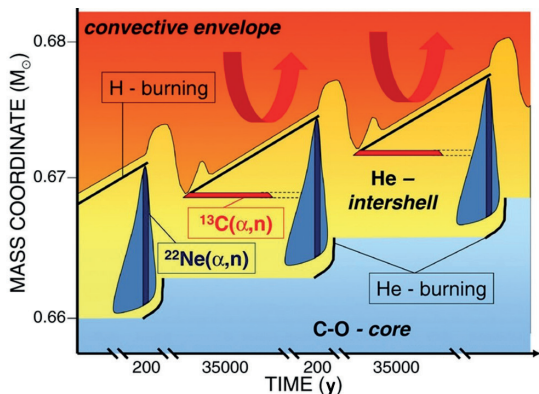
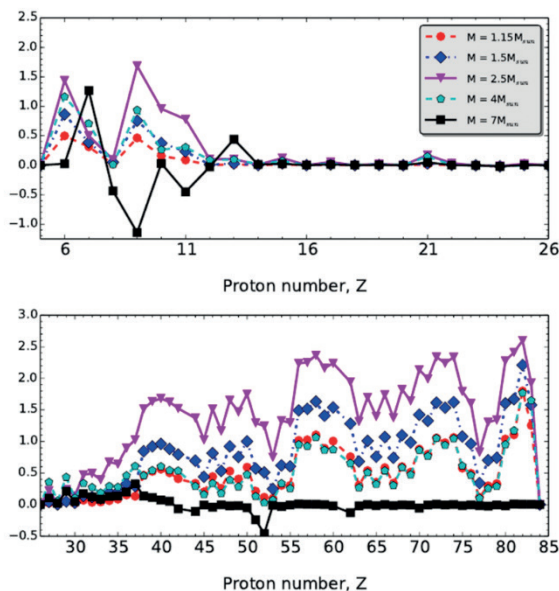


Fig. 4: Working of the s-process in low and intermediate-mass stars with an initial mass of less than $8 M_{\odot}$. $^{13}\text{C}(\alpha, n)^{16}\text{O}$ is active in the interpulse period on timescales of more than 10^5 years, while $^{22}\text{Ne}(\alpha, n)^{25}\text{Mg}$ acts only during the He-flash, on timescales of years (left panel adapted from REIFARTH ET AL. 2014). The result is dependent on the stellar mass. The process is most active for stars around $2.5 M_{\odot}$, as can be noticed in the right panel (from KARAKAS & LATTANZIO 2014), showing the resulting abundance pattern at the end of the stellar life which is blown off in the planetary nebular phase (see Fig. 6 in part I). The overall solar s-process abundances are the result of a superposition of contributing stellar masses, and also of



the initial stellar metallicities $[\text{Fe}/\text{H}]$. For a “secondary process”, acting on pre-existing inherited seed abundances like Fe, the latter influence the n/seed ratios and determines the effectiveness of the process. Both aspects come close to an exponential superposition of neutron exposures τ_n , as shown in Fig. 3 (right panel).

to the fact that the H- and He-burning shells are located within a small distance. Both do not burn in a constant fashion. If the H-burning zone is on, it creates He fuel. After sufficient He is produced, He is ignited in an unburned He-rich zone (at sufficient densities and temperatures). The burning is not stable, the amount of energy created in a shallow zone is not sufficient to lift the overlaying H-shell which could cause expansion and cooling, i.e. steady burning. Instead, He-burning, being dependent on the density squared due to the $^4\text{He}(2\alpha, \gamma)^{12}\text{C}$ reaction, burns almost explosively (in a flash), causing then a stronger expansion which even stops H-burning in the H-shell.

s-process sites:

As discussed above, the mass region up to $A \approx 90$ can result from the neutron exposures found in central He-burning of massive stars (the weak s-process) with neutrons released from the $^{22}\text{Ne}(\alpha, n)^{25}\text{Mg}$ reaction, discovered as neutron source by CAMERON (1960). For making elements as heavy as Pb and Bi more efficient neutron sources are required. The s-process (moving along stability) cannot go beyond these elements as it hits regions of alpha-decay. Neutron captures will populate nuclei above the alpha-emission threshold, and these (n, α) reactions go back to a reduced mass number $A - 3$. The s-process in low and intermediate mass stars (the main s-process component) takes place due

expansion which even stops H-burning in the H-shell.

This behavior repeats in recurrent flashes, first introduced by SANDERS (1967), extended by ULRICH & SCALO (1972), IBEN & TRURAN (1978), and many further investigations (for reviews see KÄPPELER ET AL. 1989, 2011, KARAKAS & LATTANZIO 2014, BISTERZO ET AL. 2017). H is mixed into the unburned He fuel, causing the $^{12}\text{C}(p, \gamma)^{13}\text{N}(\beta^+)^{13}\text{C}(\alpha, n)^{16}\text{O}$ reaction sequence (discovered as neutron source by CAMERON 1955) and the production of neutrons in a more efficient way than only via $^{22}\text{Ne}(\alpha, n)^{25}\text{Mg}$. This behavior is shown in Fig. 4. Being dominantly based on experimental nuclear input along stable nuclei, with few exceptions for branchings, such su-

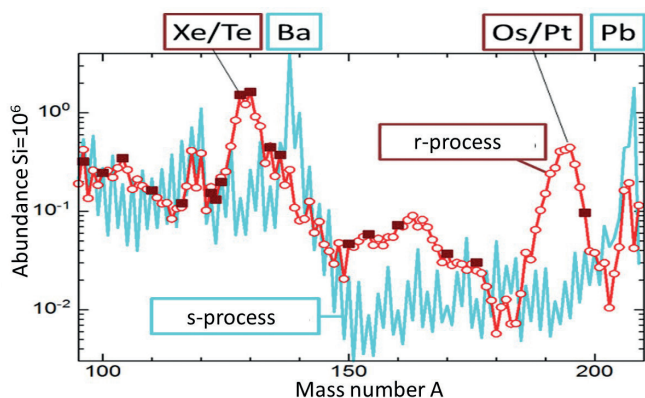
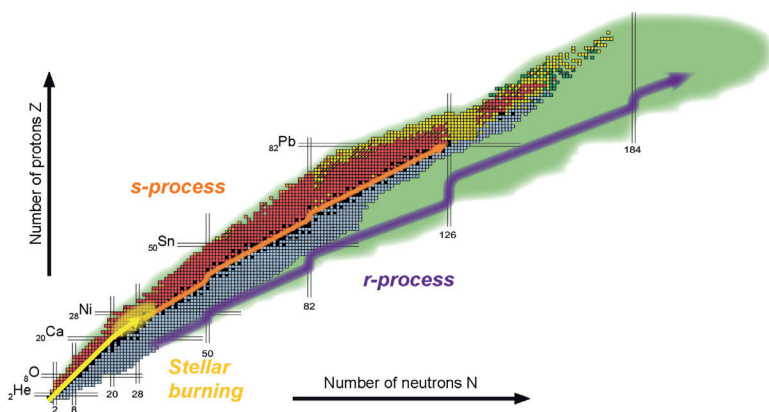


Fig. 5: left panel (adapted from COWAN & THIELEMANN 2004), solar s-process abundances (blue) resulting from a superposition of stellar s-process sources (ARLANDINI 1999) which fit the solar abundances of pure s-process nuclei. The subtraction from global solar abundances provides the abundance contributions due to the remaining processes which create heavy nuclei up to the actinides, mainly the before-mentioned and later discussed r-process. The right panel (courtesy of EMMI, GSI/Different Arts) shows the nuclear chart with major nucleosynthesis processes, from the formation of elements up to Fe, Ni, Zn in fusion reactions during stellar evo-



lution and explosions, the s-process path along stability up to Pb and Bi, and the (later to be discussed) r-process path. Stable nuclei are indicated by black squares, experimentally known β^+ -unstable nuclei by red squares, β^- -unstable nuclei by blue squares, alpha-unstable nuclei by yellow squares. The borders of unstable nuclei, stable against neutron or proton emission (predicted by nuclear mass models) appear in a light green shade. Horizontal or vertical lines stand for neutron or proton shell closures, $N = 8, 20, 28, 50, 82, 126, 184$ and $Z = 8, 20, 26, 28, 50, 82$. $Z = 114$ is not shown here.

perpositions in τ_n can permit a fit to the solar abundances of pure s-process nuclei, predicting also the s-process contributions of all other nuclei.

Subtracting the overall s-process contributions from the solar abundances of heavy elements, permits a safe way to predict the contributions required from other processes (see Fig. 5). In order to obtain a high precision for these predictions a high degree of precision for the s-process contributions is necessary.

The progress over the years has been enormous, starting with many contribution from the reactor community, e.g. MACKLIN & GIBBONS (1965) over BAO ET AL. (1987, 2000) to the reviews by REIFARTH ET AL. (2014) and DOMINGO-PARDO ET AL. (2020) with precisions in most cases on the percent level, but in a few cases for very small cross sections reaching up to 20 %. A further issue is that the two neutron sources $^{13}\text{C}(\alpha, n)^{16}\text{O}$ and $^{22}\text{Ne}(\alpha, n)^{25}\text{Mg}$ act under different conditions (e.g. dominantly during the interpulse phase, requiring cross section measurement close to 8 keV, or in the He-flash phase, requiring cross section measurement close to 30 keV). If aiming for precision determinations of neutron capture rates on the percent level, this is important to consider, although neutron capture rates vary only slightly with environment temperatures, as discussed in part I. Nevertheless, the precision reached by now permits a highly accurate determination of abundance contributions to heavy elements from the remaining processes. **s-process sites:** *We have to separate the s-process contributions from the weak s-process (dominated by core He-burning of massive stars) and the main s-process, being essentially due to the intertwined He and H-shell burning and flashes of low and intermediate mass stars, as can be seen in the right panel of Fig. 3 and in Fig. 4. In addition, the s-process, acting on pre-existing Fe-group elements from previous generations of stars, is a so-called secondary process, and therefore dependent on the metallicity [Fe/H].*

The r-process:

The s-process ends at Pb, Bi and some short-lived Po isotopes. Essentially all heavier elements up to the actinides have to be produced in the r-process. The major question is whether this process is determined by unique conditions in one specific astrophysical environment, or whether it also results from a superposition of conditions. We will defer this question to the point when we go into specific scenarios. At present we just assume that one has conditions which result in much higher neutron densities than in the s-process, which were presented above and range from $n_n = 10^7 \text{ cm}^{-3}$ in the interpulse phase to a few times 10^{10} cm^{-3} in the He-flash pulses. Fig. 6 (upper panel) shows simple calculations when samples of solar system abundance of ^{126}I or ^{235}U and ^{238}U are exposed to a neutron density of $n_n \approx 6 \times 10^{18} \text{ cm}^{-3}$. One sees that for such conditions typical neutron capture timescales are of the order 10^{-4} s (the presented calculations are limited to isotopic chains which end at ^{131}I and ^{245}U). These time scales go inversely with the neutron density, thus leading to 10^{-6} s for $n_n \approx 6 \times 10^{20} \text{ cm}^{-3}$. Therefore, high neutron densities cause exceedingly fast neutron captures in isotopic chains in comparison to beta-decay half-lives of the isotopes involved. Inverse photo-disintegrations win against capture reactions when $kT > Q/30$. We noticed in part I and the beginning of the present part II that this is the case for

$T > (5 - 6) \times 10^9 \text{ K}$ when involving reactions with Q -values of the order 10 - 12 MeV among stable nuclei. For highly neutron-rich nuclei far from beta-stability with neutron separation energies S_n (the Q -value of the reverse neutron capture) of the order 2 MeV, this requires only temperatures slightly above 10^9 K . If in this way a chemical equilibrium between neutron captures and photodisintegrations is attained in a complete isotopic chain, a maximum abundance, resulting from the competition of neutron captures and reverse photodisintegrations, will occur for a specific isotope with an $S_n = f(n_n, T)$. This is the same S_n in all isotopic chains, characterizing an r-process path. The chains in chemical equilibrium are connected by beta-decays from Z to $Z + 1$. This concept, called the waiting-point approximation, was introduced already by BURBIDGE ET AL. (1957) and CAMERON (1957). The positions of the waiting points are only depend-

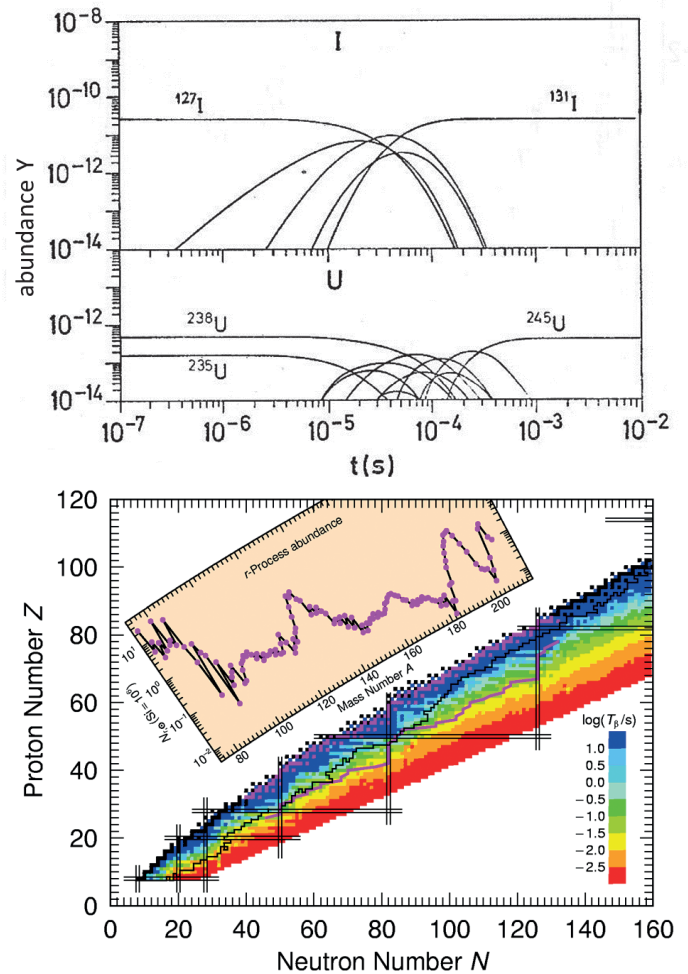


Fig. 6: upper panel, When starting with solar abundances of ^{127}I , ^{235}U and ^{238}U in a plasma with a neutron density of $6 \times 10^{18} \text{ cm}^{-3}$ and a temperature of 10^9 K , neutron captures take typically 10^{-4} s or less to end up at the limiting mass number utilized in the nuclear network. Such neutron capture life times change linearly with the inverse neutron density. Under such conditions neutron captures precede until they are balanced by inverse photodisintegrations. The lower panel (from KRATZ ET AL. 1993) indicates such an r-process path with a neutron separation energy of about 2 MeV. Such a contour line of constant S_n displays kinks at neutron shell closures. The color-coded beta-decay half-life predictions show that the path passes through the longest half-lives at the top of these kinks, consequently resulting in abundance peaks at mass number A (after beta-decay back to stability) which represent the position of the kinks far from stability rather than nuclei with closed neutron shells at stability. The magenta path runs through regions of beta-decay half-lives in the range of 10^1 to 10^2 s , clearly longer than the neutron capture lifetimes seen in the top panel of this figure.

ent on nuclear masses, related to the equilibrium $S_n(n_n, T)$, as shown in Fig. 5. The smaller S_n of the path, the more neutron-rich are the nuclei involved. This requires a high n_n and neutron-richness of matter, or equivalently a small Y_e (the overall proton to nucleon ratio).

Presently a number of large-scale nuclear facilities like GSI/FAIR in Darmstadt, FRIB in Michigan, RIKEN in Tokyo, Lanzhou in China are having great successes reaching far out to highly beta-unstable neutron-rich nuclei (HOROWITZ ET AL. 2019, COWAN ET AL. 2021) and aim to reach the path also for the heaviest nuclei. However, an r-process path with $S_n \approx 2$ MeV is presently still largely moving in experimentally unknown territory and one has to rely on theoretical predictions (see right panel of Fig. 5).

History and r-process sites:

Part I discussed the progress over the years in predicting nucleosynthesis processes and sites for elements up to the Fe-group (with an addition related to type Ia supernovae in the beginning of this part II). The understanding how the different stellar contributions enter the “chemical evolution” for light and intermediate mass elements in our Galaxy (see Fig. 2 in part I) evolved from MATTEUCCI & GREGGIO (1986) to NOMOTO ET AL. 2013, PRANTZOS ET AL. (2018) and KOBAYASHI ET AL. (2020). While the pioneering papers of BURBIDGE ET AL. (1957) and CAMERON (1957) laid out also the underlying nuclear physics of the rapid neutron capture r-process responsible for the heaviest elements in the Universe, the site was still unclear. For many years the subject gained maturity by improving nuclear input, astrophysical modeling, and observational efforts (from SEEGER ET AL. 1965, HILLEBRANDT 1978, COWAN ET AL. 1991, KRATZ ET AL. 1993, PFEIFFER ET AL. 2001, ARNOULD ET AL. 2007, QIAN & WASSERBURG 2007, FAROUQI ET AL. 2010, ROEDERER ET AL. 2010, KRATZ ET AL. 2014 to COWAN ET AL. 2021), starting from neutron density superpositions via adiabatic expansions of matter for a given Y_e , entropy S , and expansion time scale τ , to realistic astrophysical scenarios. Only in recent years these became more concrete, including neutron star mergers (e.g. FREIBURGHaus ET AL. 1999, JUST ET AL. 2015, BAUSWEIN ET AL. 2017, THIELEMANN ET AL. 2017, ROSSWOG ET AL. 2018, SHIBATA & HOTOKEZAKA 2019), magneto-rotational jet supernovae (e.g. WINTELER ET AL. 2012, MÖSTA ET AL. 2018, NISHIMURA ET AL. 2017, REICHERT ET AL. 2021), and collapsars (fast rotating massive stars whose final core-collapse ends in a black hole and mass ejection from jets and disks, see SIEGEL ET AL. 2019; SIEGEL 2019). The first site is related to stellar evolution (and explosions) in binary systems (see also the beginning of this part II), while the latter two options are both related to the final collapse of massive stars (see Fig. 9 of part I). The original idea was that regular core collapse supernovae could be responsible for a strong r-process, i.e. reproducing solar r-process abundances (e.g. WOOSLEY ET AL. 1994; TAKAHASHI ET AL. 1994), also up to the heaviest nuclei, within a high-entropy neutrino-powered wind. Recent supernova simulations, however, do not support the required conditions and it seems that, if at all, supernovae could only lead to a weak r-process, not producing the heavy r-process nuclei in solar proportions (ROBERTS ET AL. 2012, MARTÍNEZ-PINEDO ET AL. 2012, WU ET AL. 2014, FISCHER ET AL. 2020a). Quark-deconfinement (QD) supernovae (FISCHER ET AL. 2020b) were suggested as another weak r-process site (see Fig. 9 of part I).

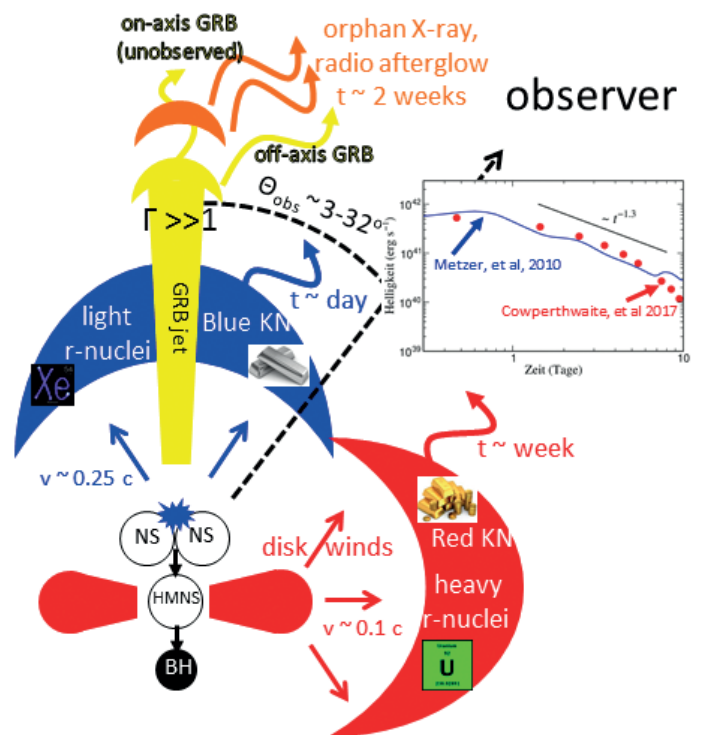
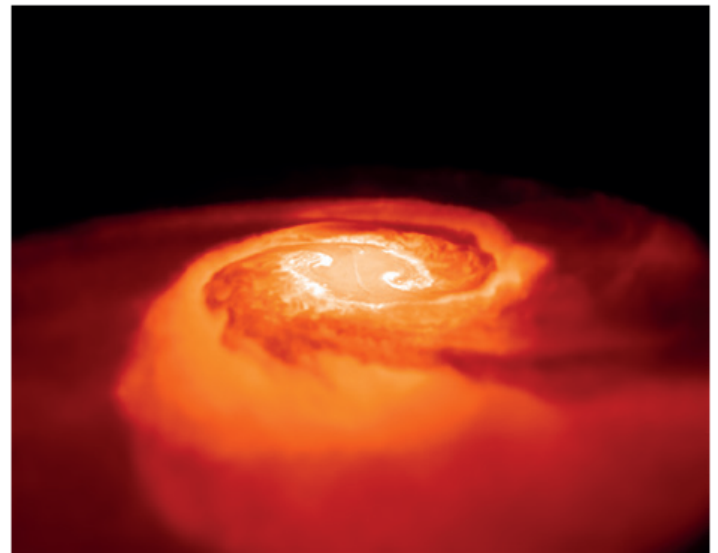


Fig. 7: upper panel, a temperature distribution plot from a neutron star merger simulation (courtesy of S. Rosswog). In the early phase the collision leads to a hot central region and “tidal” mass ejecta in terms of spiral arms. Lower panel (courtesy of B. Metzger), the central merged object is (although beyond the stable neutron star mass limit) initially supported by thermal and rotational energy and forms a hypermassive neutron star which blows off a neutrino powered wind, as in core-collapse supernovae, preferentially in axis direction. After the formation of the black hole an accretion disks forms which leads to axial jets (causing a gamma-ray burst with very large Lorentz factors Γ) and horizontal accretion disk outflows. The tidal (almost pristine) very neutron-rich ejecta and the accretion disk outflows form the heaviest elements. The neutrino-powered wind increases the (initially very low) Y_e from values < 0.1 up to possibly 0.3 via neutrino captures on neutrons ($\nu+n \rightarrow p+e$), which causes only a weak r-process and less massive nuclei. Due to the higher density of electronic states in the heaviest elements (lanthanides and actinide) photonic radiation transport leads to a red appearance of the hot object, while the intermediate to light heavy elements cause an appearance in blue light.

While most of the suggested sites are based on modeling alone (possibly permitting indirect identifications in abundances of low-metallicity stars), only neutron star mergers are robustly, and by direct observations of the event itself,

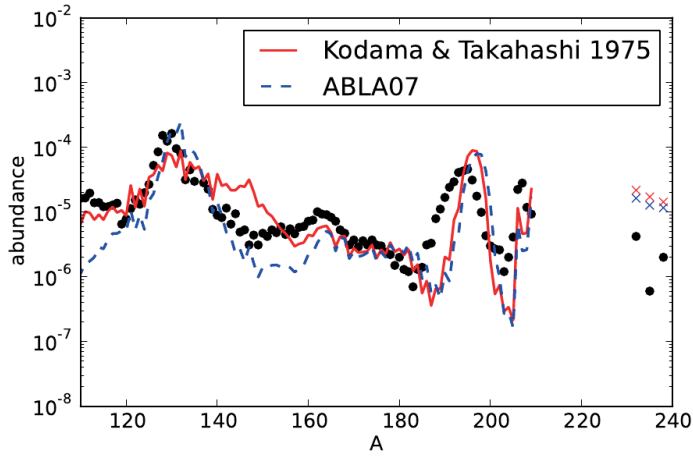
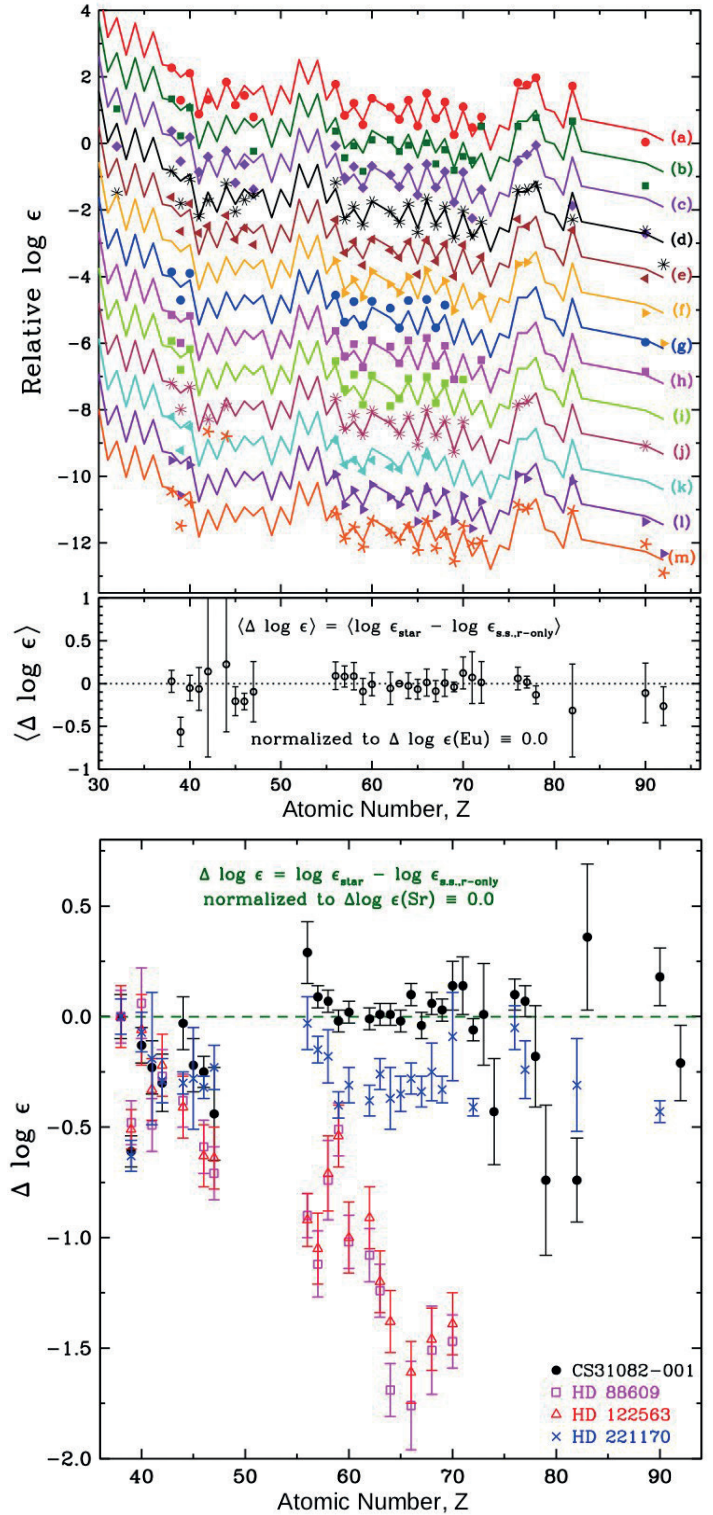


Fig. 8: top left (from EICHLER ET AL. 2015); solar r -process abundances, black dots, as defined in Fig. 5 (left panel) by the difference of solar abundances and solar s -process abundances, compared to results of neutron star merger nucleosynthesis simulations (from the tidal arm ejecta only, i.e. without contributions from neutrino winds of the intermediately existing hypermassive neutron star and outflows of the accretion disk surrounding the final black hole). The very neutron-rich conditions ($Y_e < 0.1$) lead to a strong influence of fission, cycling matter back to the $A = 130$ peak and being affected by the choice of predicted fission fragment distributions (indicated by ABLA and Kodama). The influence of fission and related neutron release in the final phases permits neutron captures to shift the abundances around $A = 195$ to higher mass numbers. Therefore, even in the same object, a superposition of conditions is required to obtain an overall solar r -process fit. Top right (from COWAN ET AL. 2021); logarithmic (arbitrarily shifted) abundances of heavy elements in “low metallicity stars” with $[Fe/H] < -2.5$, i.e. stars born in the early galaxy before s -process contributions by low and intermediate mass stars emerged, exhibiting an r -process pattern. The solid lines, standing for a solar r -process distribution of elements as function Z (not A), underline a very close to solar r -pattern, with some deviations for lighter heavy elements and the heaviest ones. Bottom (from COWAN ET AL. 2021); the abundance pattern of four specific stars: two limited- r or weak r -process stars, which do not exhibit abundances in the $A = 195$ peak, and two r -process-rich stars (corresponding to the cases d and e in the top right panel and behaving like the majority of that display). There exist also so-called “actinide-boost stars” which show enhanced abundances of U and Th. The limited- r stars and actinide boost stars point to other sites than neutron star mergers. The limited- r stars go probably back to rare types of supernovae shown in Fig. 9 of part I, the actinide boosts require an important fraction of ejecta with $Y_e = 0.1 - 0.15$, probably due to an equilibrium of weak interactions (electron and reverse neutrino captures) in the inner disk of black hole accretions disks, pointing to collapsars or neutron star mergers with a large combined mass, causing fast black hole formation after the merger (see METZGER ET AL. 2019, COWAN ET AL. 2021), rather than an intermediately existing hypermassive neutron star, in which the neutrino wind would lift Y_e to higher values with a less powerful r -process.

connected to r -process production. The follow-up of the gravitational wave event GW170817 (ABBOTT ET AL. 2017) revealed strong electromagnetic emission in the aftermath of the merger (EVANS ET AL. 2017, KASLIWAL ET AL. 2019, WU ET AL. 2019) and showed in particular the expected signatures of an r -process powered “kilonova” (see Fig. 7). The decay of its bolometric light curve agreed well with the expectations for radioactive heating rates from a broad range of r -process elements (e.g. METZGER ET AL. 2010, ROSSWOG ET AL. 2018, ZHU ET AL. 2018, METZGER 2019). The early blue and the late (infra-)red emissions point to the production of weak (lanthanide-free) r -process ejecta from the neutrino wind (substantiated also by the spectral detection of Sr,



WATSON ET AL. 2019) as well as heavy (lanthanides and beyond) r -process ejecta. This heavy r -process is the result of decompressing neutron star matter from its initial, very low $Y_e (< 0.1)$, LATTIMER ET AL. 1977, FREIBURGHANUS ET AL. 1999, KOROBKIN ET AL. 2012, EICHLER ET AL. 2015). Variations in nucleosynthesis conditions are described in WANAJO ET AL. (2014), JUST ET AL. (2015), MARTIN ET AL. (2015), WU ET AL. (2016), BAUSWEIN ET AL. (2017), THIELEMANN ET AL. (2017), MILLER ET AL. (2019). In summary, there is strong evidence that neutron star mergers produce a broad, and maybe the whole, r -process range.

As seen in Fig. 8 (bottom panel), observations of low metallicity stars indicate the existence of a weak or limited r -process, while most r -process enhanced stars show a solar r -process pattern (top right panel). This goes together with

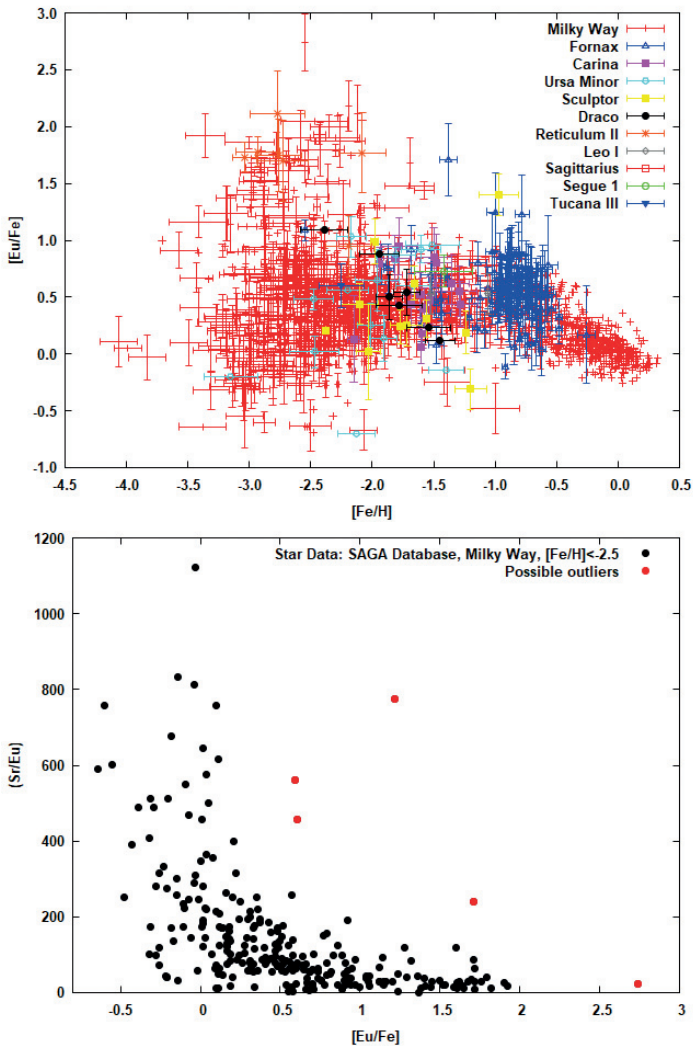


Fig. 9: $[Eu/Fe]$ vs. $[Fe/H]$ and $[Sr/Eu]$ vs. $[Eu/Fe]$ (from the SAGA data base, SUDA ET AL. 2008, courtesy of K. Farouqi). For metallicities in the range of -2 to 0 it can be seen that $[Eu/Fe]$ behaves like alpha-elements of Fig. 2 in part I, as if Eu would originate from core-collapse supernovae, and the increased Fe production in (delayed) type Ia supernovae causes the decline to solar ratios ($[Eu/Fe] = 0$ at $[Fe/H] = 0$). However, for low metallicity stars in the range $[Fe/H] < -2$ a large scatter can be identified which points to rare events with large ejecta amounts, causing an inhomogeneous spatial distribution in the interstellar medium out of which new stars are born (all red data points refer to Milky Way stars, the colored ones to nearby dwarf galaxies). The lower panel shows that for low $[Eu/Fe]$ values the $[Sr/Eu]$ ratio rises strongly, indicating a weak r-process with a strongly tilted abundance pattern as shown in the bottom panel of Fig. 8.

a variation of e.g. the Sr/Eu ratio, ranging from about 1120 down to 0.5 (HANSEN ET AL. 2018), and indicating the different decline of the abundance curve as a function of A . Some of the r-process enriched stars show an "actinide boost", i.e. their Th or U to Eu ratio is supersolar (e.g. ROEDERER ET AL. 2010, HOLMBECK ET AL. 2018, 2019).

Another result from the observation of low-metallicity stars is that especially Eu, with reasonably easy to detect spectroscopic features, shows a large scatter in comparison to Fe (Fig. 9, top panel), much larger than the alpha elements (from O to Ti, see Fig. 2 part I) which go back to core-collapse supernova nucleosynthesis. This points to the strong r-process being a very rare event, occurring with a frequency smaller than that of supernovae by a factor of 100 to 1000. Similar features can also be seen for Ag and Pd (HANSEN ET AL. 2012) as well as Mo and Ru (MISHENINA ET AL. 2019).

This is underlined by the detection/non-detection of ^{60}Fe (a supernova product) vs. ^{244}Pu in deep-sea sediments (e.g. WALLNER ET AL. 2015; HOTOKEZAKA ET AL. 2015).

Summarizing the discussion above: we have a number of suggested r-process sites, but only one of them is proven by a direct observation of the explosive event. Observations of low metallicity stars show essentially three types of patterns, a weak or limited r-process, a strong solar-type r-process, and an actinide-boosted r-process (for reviews and impact on galactic chemical evolution see e.g. WEHMEYER ET AL. 2015, VAN DE VOORT ET AL. 2020, COWAN ET AL. 2021). Whether the latter two types are produced in different sites or result from variations within the same site (e.g. neutron star mergers) is still debated. The question is now how to identify features which can point back to individual sites. A promising approach is to look for correlations among different elements. COWAN ET AL. (2005) compared the abundances of Fe, Ge, Zr, and r-process Eu in low metallicity stars. They found a strong correlation of Ge with Fe, indicating the same nucleosynthesis origin (core-collapse supernovae), a weak correlation of Zr with Fe, indicating that other sites than regular core-collapse supernovae (without or with low Fe-ejection) contribute as well, and no correlation between Eu and Fe, pointing essentially to a pure r-process origin with negligible Fe-ejection. More recent data from the SAGA and JINA databases (SUDA ET AL. 2008, ABOHALIMA & FREBEL 2018) permit a correlation between Eu and Fe for $[Eu/Fe] < 0 - 0.3$, i.e. for stars with lower than average r-process enrichment which also show high $[Sr/Fe]$ values (Fig. 9, lower panel). Interpreted in a straight-forward way this would point to a negligible Fe/Eu ratio (in comparison to solar ratios) in the major r-process sources (like neutron star mergers and collapsars), while a noticeable co-production of Fe with Eu is possible in less strong r-process sources, e.g. with a weak r-process (probably pointing to rare supernova types).

Other processes which might add matter to trans-Fe elements or isotopes:

Before ending this section, one should consider that the so-called solar r-process abundances, obtained by subtracting solar s-process abundances from solar abundances (see e.g. ARLANDINI ET AL. 1999; KÄPPELER ET AL. 2011; PRANTZOS ET AL. 2020), might combine a number of different contributions. Especially the light trans-Fe elements like Sr, Y, Zr, seem to have also other origins aside from the typical r-process (TRAVAGLIO ET AL. 2004, FRÖHLICH ET AL. 2006, FAROUQI ET AL. 2009, HANSEN ET AL. 2012, EICHLER ET AL. 2018) which could possibly be attributed to regular core-collapse supernovae. We discussed in part I already the **νp -process**, taking place in the innermost ejecta of core-collapse supernovae. These mass zones are strongly irradiated by (electron) neutrinos and anti-neutrinos as pointed out below Fig. 8 in part I. The related capture reactions on neutrons and protons determine the overall neutron/proton ratio in matter, and for similar neutrino and antineutrino energies proton abundances win over neutron abundances, resulting in a $Y_e > 0.5$ (FRÖHLICH ET AL. 2006). This permits to produce a number of nuclei beyond the Fe-group by a sequence of proton captures and beta-decays. This ends at ^{64}Ge , which has a half-life of 64 s, too long to permit a build-up of heavier nuclei in explosive environments. However, this can be bridged by the faster $^{64}\text{Ge}(n,p)^{64}\text{Ga}$ reaction (with neutrons produced via antineutrino capture on free protons in the

slightly proton-rich environment) and subsequent production of proton-rich nuclei up to Sr and maybe $A \approx 90 - 100$. Proton-rich nuclei which cannot be produced via an s-process path (as ^{84}Sr in Fig. 3) can be made in such a way and even amount to isotopic fractions of the order 10 % in the Mo and Ru isotopes. Heavier proton-rich so-called ***p- or γ -process*** isotopes (with isotopic fractions of only about 1 %) can be generated in core-collapse as well as type Ia supernova explosions, when pre-existing heavy s- or r-process isotopes are kind of “sandblasted” by hot photons and cause photo-disintegrations with such reaction endpoints (see HOWARD ET AL. 1991, RAYET ET AL. 1995, TRAVAGLIO ET AL. 2011, RAUSCHER ET AL. 2013, PIGNATARI ET AL. 2016, BATTINO ET AL. 2020). Last, but not least, another (for the overall abundance pattern less important) process should be mentioned as well, the

i-process with a slightly stronger neutron source than in the s-process (initially introduced by COWAN & ROSE 1977, see for most recent aspects DENISSEKOV ET AL. 2021).

This has been a long and maybe (but hopefully not) fatiguing journey through the chart of nuclei and periodic table of the elements, but hopefully it gave an impression how we arrived at the abundance pattern of elements and isotopes on earth, in the solar system, the Milky Way and the Universe. This might be aided with two final plots.

Bibliography:

- Abbott, B. P. et al. 2017, Phys. Rev. Lett. **119**, 161101
 Abohalima, A. Frebel, A. 2018, Astrophys. J. Suppl. **238**, 36
 Arlandini, C. et al. 1999, Astrophys. J. **525**, 886
 Arnett, W. D. 1969, Astrophys. Space Sci. **5**, 180
 Arnett, W. D. Truran, J. W., Woosley, S. E. 1971, Astrophys. J. **165**, 87
 Arnould, M., Goriely, S., Takahashi, K. 2007, Phys. Rep. **450**, 97
 Bao, Z. Y., Käppeler, F., 1987, At. Data Nucl. Data Tables **36**, 411
 Bao, Z. Y., Beer, H., Käppeler, F., Voss, F., Wisshak, W., Rauscher, T. 2000, At. Data Nucl. Data Tables **76**, 70
 Bauswein, A., Just, O., Janka, H.-T., Stergioulas, N. 2017, Astrophys. J. Lett. **850**, L34
 Battino, U. et al. 2020, MNRAS **497**, 4981
 Bisterzo, S., Travaglio, C., Wiescher, M., Käppeler, F., Gallino, R. 2017, Ap. J. **835**, 97
 Burbidge, E. M., Burbidge, G. R., Fowler, W. A., Hoyle, F. 1957, Rev. Mod. Phys. **29**, 547
 Cameron, A. G. W. 1955, Astrophys. J. **121**, 144
 Cameron, A. G. W. 1957, Publ. Astron. Soc. Pac. **69**, 201; Astron. J. **62**, 9; Chalk River Report 41 (republished in Dover Publications, New York, 2013)
 Cameron, A. G. W. 1960, Astron. J. **65**, 485
 Cameron, A. G. W. 2003, Astrophys. J. **587**, 327
 Cowan, J. J., Rose, W. K. 1977, Astrophys. J. **212**, 149
 Cowan, J. J., Thielemann, F.-K., Truran, J. W. 1991, Phys. Rep. **208**, 267
 Cowan, J. J., Thielemann, F.-K. 2004, Physics Today **57**, 47
 Cowan, J. J., Sneden, C., Beers, T. C., et al. 2005, Astrophys. J. **627**, 238
 Cowan, J. J., Sneden, C., Lawler, J. E., Aprahamian, A., Wiescher, W., Langanke, K., Martinez-Pinedo, G., Thielemann, F.-K. 2021, Rev. Mod. Phys. **93**, 015002
 Cyburt, R. H. et al. 2010, Astrophys. J. Suppl. **189**, 240
 Dan, M., Guillochon, J., Brüggem, M., Ramirez-Ruiz, E., Rosswog, S. 2015, MNRAS **454**, 4411
 Denissenkov, P. A., Herwig, F., Perdikakis, G., Schatz, H. 2021, MNRAS **503**, 3913
 Domingo-Pardo, C. et al. 2020, J. of Phys.: Conf. Series 1668, 012013
 Eichler, M., Arcones, A., Kelic, A., Korobkin, O. et al. 2015, Astrophys. J. **808**, 30
 Eichler, M., Nakamura, K., Takiwaki, T., et al. 2018, J. Phys. G: Nucl. Part. Phys. **45**, 014001
 Evans, P. A. et al. 2017, Science **358**, 1565
 Farouqi, K., Kratz, K., Pfeiffer, B., et al. 2010, Astrophys. J. **712**, 1359
 Fischer, T., Guo, G., Dzhiyev, A. A., et al. 2020a, Phys. Rev. C, **101**, 025804
 Fischer, T., Wu, M.-R., Wehmeyer, B., Bastian, N.-U., Martinez-Pinedo, G., Thielemann, F.-K. 2020b, Astrophys. J. **894**, 9

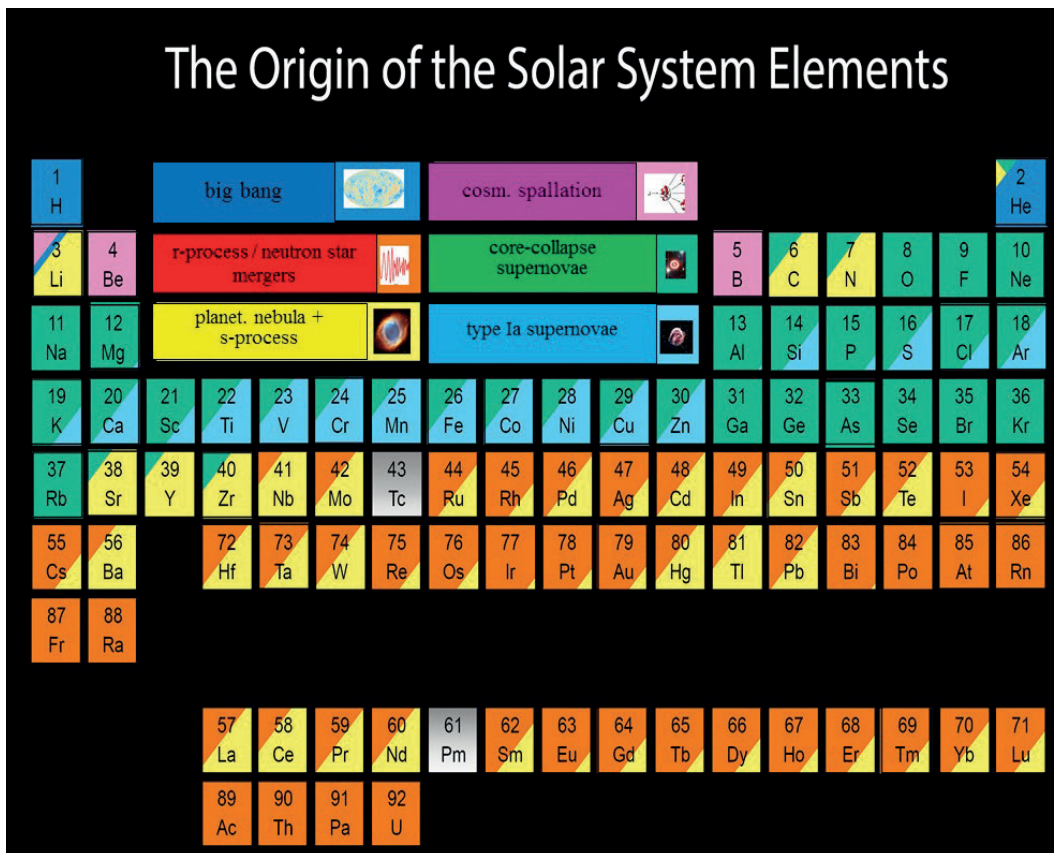
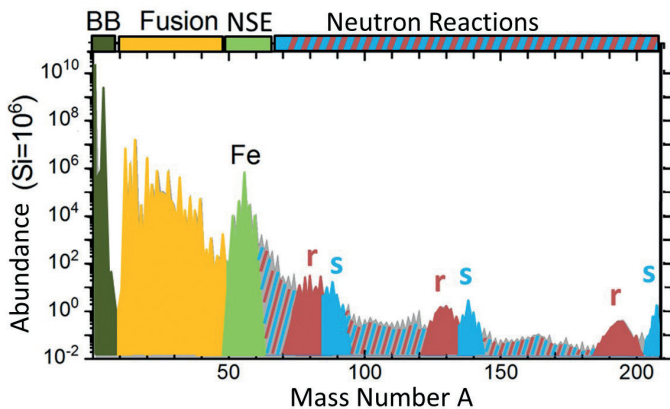


Fig. 10: upper panel (courtesy of F. Käppeler); solar abundances as a function of mass number A , divided in the responsible processes from big bang nucleosynthesis, fusion reactions in the evolution of stars and their explosions, including conditions which lead to a full chemical equilibrium of abundances for nuclei with the highest binding energies (nuclear statistical equilibrium NSE), and s- and r-process contributions. The abundances of p-nuclei are too small to be visible in this plot. Lower panel (courtesy of J. Johnson): the periodic table of the elements where the processes of the upper panel are translated into stellar sites. It should be noticed that s- and r-process should be divided into weak and main components, where the weak components are related to different sites than indicated in the plot, like massive stars and rare classes of supernovae.

- Freiburghaus, C., Rosswog, S., Thielemann, F.-K. 1999, *Astrophys. J.*, **525**, L121
- Fröhlich, C., Martínez-Pinedo, G., Liebendörfer, M., Thielemann, F.-K. et al. 2006, *Phys. Rev. Lett.* **96**, 142502
- García-Senz, D., Cabezón, R. M., Domínguez, I., Thielemann, F.-K. 2016, *Astrophys. J.* **819**, 132
- Goldstein, D. A., Kasen, D. 2018, *Ap. J. Lett.* **852**, L33
- Gronow, S., et al. 2021, arXiv:2103.14050
- Hansen, C. J., Primas, F., Hartman, H., et al. 2012, *Astron. & Astrophys.* **545**, A31
- Hansen, T. T., Holmbeck, E. M., Beers, T. C., et al. 2018, *Astrophys. J.* **858**, 92
- Hillebrandt, W. 1978, *Space Sci. Rev.* **21**, 639
- Hillebrandt, W., Kromer, M., Röpke, F. K., Ruiter, A. J. 2013, *Frontiers of Physics* **8**, 116
- Höfllich, P., Wheeler, J. C., Thielemann, F.-K. 1998, *Astrophys. J.* **495**, 617
- Höfllich, P. et al. 2017, *Astrophys. J.* **846**, 58
- Holmbeck, E. M., Sprouse, T. M., Mumpower, M. R., et al. 2019, *Astrophys. J.* **870**, 23
- Horowitz, C. J. et al. 2019, *J. of Physics G: Nuclear and Particle Physics* **46**, 083001
- Hotokezaka, K., Piran, T., Paul, M. 2015, *Nature Physics* **11**, 1042
- Howard, W. M., Meyer, B. S., Woosley, S. E. 1991, *Astrophys. J.* **373**, L5
- Hoyle, F., Fowler, W. A. 1960, *Astrophys. J.* **132**, 565
- Iben, I. Jr., Truran, J. W. 1978, *Astrophys. J.* **220**, 980
- Iben, I. Jr., Tutokov, A. V. 1984, *Astrophys. J. Suppl.* **54**, 335
- Jiang J. A. et al. 2017, *Nature* **550**, 80
- José, J. 2016, 2020, *Stellar Explosions*, in *Series in Astronomy & Astrophysics*, Taylor & Francis, CRC Press
- Just, O., Bauswein, A., Pulpillo, R. A., Goriely, S., Janka, H.-T. 2015, *MNRAS* **448**, 54
- Käppeler, F., Beer, H., Wisshak, K. 1989, *Rep. Progr. Phys.* **52**, 945
- Käppeler, F., Gallino, R., Bisterzo, S., Aoki, W. 2011, *Rev. Mod. Phys.* **83**, 157
- Karakas, A. I., Lattanzio, J. C. 2014, *Publ. Astron. Soc. Australia* **31**, e030
- Kasliwal, M. M., Kasen, D., Lau, R. M., et al. 2019, *MNRAS* slz007
- Khokhlov, A., Müller, E., Höfllich, P. 1993, *Astron. & Astrophys.* **270**, 223
- Kobayashi, C., Karakas, A. I., Lugaro, M. 2020, *Astrophys. J.* **900**, 179
- Korobkin, O., Rosswog, S., Arcones, A., Winteler, C. 2012, *MNRAS* **426**, 1940
- Kratz, K.-L., Bitouzet, J., Thielemann, F.-K., Möller, P., Pfeiffer, B. 1993, *Astrophys. J.* **403**, 216
- Kratz, K.-L., Farouqi, K., Möller, P. 2014, *Astrophys. J.* **792**, 6
- Lach, S. et al. 2020, *Astron. & Astrophys.* **644**, A118
- Lamb, S. A., Howard, W. M., Truran, J. W., Iben, I., Jr. 1977, *Astrophys. J.* **217**, 213
- Lattimer, J. M., Mackie, F., Ravenhall, D. G., Schramm, D. N. 1977, *Astrophys. J.* **213**, 225
- Leung, S.-C., Nomoto, K. 2018, *Astrophys. J.* **861**, 143
- Macklin, R. L., Gibbins, J. H. 1965, *Rev. Mod. Phys.* **37**, 166
- Maeda, K., Röpke, F. K., Fink, M., Hillebrandt, W., Travaglio, C., Thielemann F.-K. 2010, *Astrophys. J.* **712**, 624
- Maeda, K., Terada, Y. 2016, *Int. J. Mod. Phys. D* **25**, 1630024
- Maoz, D., Mannucci, F., Nelemans, G. 2014, *Ann. Rev. Astron. Astrophys.* **52**, 107
- Martin, D., Perego, A., Arcones, A., et al. 2015, *Astrophys. J.* **813**, 2
- Martínez-Pinedo, G., Fischer, T., Lohs, A., Huther, L. 2012, *Phys. Rev. Lett.* **109**, 251104
- Matteucci, F., Greggio, L. 1986, *Astron. Astrophys.* **154**, 279
- Meisel, Z. et al. 2020, *Phys. Rev. C* **101**, 052801
- Metzger, B. D., Martínez-Pinedo, G., Darbha, S., et al. 2010, *MNRAS* **406**, 2650
- Metzger, B. D. 2019, *Living Reviews in Relativity* **23**, 1
- Miller, J. M., Ryan, B. R., Dolence, J. C., et al. 2019, *Phys. Rev. D* **100**, 023008
- Mishenina, T., Gorbaneva, T., Pignatari, M., Thielemann, F.-K., Korotin, S. A. 2015, *MNRAS* **454**, 1585
- Mishenina, T., Pignatari, M., Gorbaneva, T., et al. 2019, *MNRAS* **489**, 1697
- Mösta, P. L. et al. 2014; 2015; 2018, *Astrophys. J.* **785**, L29 ; *Nature* **528**, 376; *Astrophys. J.* **864**, 171
- Müller, E. F., Arnett, W. D. 1986, *Astrophys. J.* **307**, 619
- Nishimura, N. et al. 2017, *Astrophys. J.* **836**, L21
- Noebauer, U. M., Kromer, M., Taubenberger, S., et al. 2017, *MNRAS* **472**, 2787
- Nomoto, K. 1982, *Ap. J.* **253**, 798 ; **257**, 780
- Nomoto, K., Thielemann, F.-K., Yokoi, K. 1984, *Astrophys. J.* **286**, 644
- Nomoto, K., Kobayashi, C., Tominaga, N. 2013, *Annu. Rev. Astron. Astrophys.* **51**, 457
- Pakmor, R., Kromer, M., Taubenberger, S., Springel, V. 2013, *Astrophys. J. Lett.* **770**, L8
- Palla, M. 2021, *MNRAS* **503**, 3216
- Pfeiffer, B., Kratz, K.-L., Thielemann, F.-K., Walters, W. B. 2001, *Nucl. Phys. A* **693**, 282
- Pignatari, M., Göbel, K., Reifarth, R., Travaglio, C. 2016, *Int. J. Mod. Phys. E* **25**, 1630003
- Prantzos, N., Abia, C., Limongi, M., et al. 2018, *MNRAS* **476**, 3432
- Prantzos, N., Abia, C., Cristallo, S., Limongi, M., Chieffi, A. 2020, *MNRAS* **491**, 1832
- Qian, Y.-Z., Wasserburg, G. J. 2007, *Phys. Rep.* **442**, 237
- Rayet, M., Arnould, M., Hashimoto, M., Prantzos, N., Nomoto, K. 1995, *Astron. & Astrophys.* **298**, 517
- Rauscher, T., Dauphas, N., Dillmann, I., et al. 2013, *Rep. Progr. Phys.* **76**, 066201
- Reichert, M., Obergaulinger, M., Eichler, M., Aloy, M. Á., Arcones, A. 2021, *MNRAS* **501**, 5733
- Reifarth, R., Lederer, C., Käppeler, F. 2014, *J. Phys. G: Nuclear and Particle Physics* **41**, 053101
- Roberts, L. F., Reddy, S., Shen, G. 2012, *Phys. Rev. C* **86**, 065803
- Roederer, I. U., Cowan, J. J., Karakas, A. I., et al. 2010, *Astrophys. J.* **724**, 975
- Röpke, F. K., Sim, S. A. 2018, *Space Sci. Rev.* **214**, 72
- Rosswog, S., Liebendörfer, M., Thielemann, F.-K., et al. 1999, *Astron. & Astrophys.* **341**, 499
- Rosswog, S., Sollerman, J., Feindt, U., et al. 2018, *Astron. & Astrophys.* **615**, A132
- Sanders, R. H. 1967, *Astrophys. J.* **150**, 971
- Seeger, P. A., Fowler, W. A., Clayton, D. D. 1965, *Astrophys. J. Suppl.* **11**, 121
- Seitenzahl, I. R., Townsley, D. M. 2017, in *Handbook of Supernovae*, Springer Verlag, p. 1955
- Seitenzahl, I. R., Ghavamian, P., Laming, J. M., Vogt, F. P. A. 2019, *Phys. Rev. Lett.* **123**, 041101
- Shen, K. J., Kasen, D., Miles, B. J., Townsley, D. M. 2018, *Astrophys. J.* **854**, 52
- Shibata, M., Hotokezaka, K. 2019, *Ann. Rev. Nucl. Part. Sci.* **69**, 41
- Siegel, D. M. 2019, *Eur. Phys. J. A* **55**, 203
- Siegel, D. M., Barnes, J., Metzger, B. D. 2019, *Nature* **569**, 241
- Suda, T., Katsuta, Y., Yamada, S., et al. 2008, *Publ. Astron. Soc. Japan* **60**, 1159
- Takahashi, K., Witti, J., Janka, H.-T. 1994, *Astron. & Astrophys.* **286**, 857
- Thielemann, F.-K., Nomoto, K., Yokoi, K. 1986, *Astron. Astrophys.* **158**, 17
- Thielemann, F.-K., Eichler, M., Panov, I. V., Wehmeyer, B. 2017, *Ann. Rev. Nucl. Part. Sci.* **67**, 253
- Thielemann, F.-K., Isern, J., Perego, A., von Ballmoos, P. 2018, *Space Sci. Rev.* **214**, 62
- Timmes, F. X., Woosley, S. E., Weaver, T. A. 1995, *Astrophys. J. Suppl.* **98**, 617
- Travaglio, C., Gallino, R., Arnone, E., et al. 2004, *Astrophys. J.* **601**, 864
- Travaglio C., Hillebrandt W., Reinecke M., Thielemann F.-K. 2004, *Astron. Astrophys.* **425**, 1029
- Travaglio, C., Röpke, F. K., Gallino, R., Hillebrandt, W. 2011, *Astrophys. J.* **739**, 93
- Travaglio, C. 2018, private communication
- Tsujimoto, T., Nishimura, N. 2018, *Astrophys. J. Lett.* **863**, L27
- Ulrich, R. K., Scalo, J. M. 1972, *Astrophys. J. Lett.* **176**, L37
- van de Voort, F., Pakmor, R., Grand, R. J. J., et al. 2020, *MNRAS* **494**, 4867
- Wallner, A., Faestermann, T., Feige, J., et al. 2015, *Nature Comm.* **6**, 5956
- Wanajo, S., Sekiguchi, Y., Nishimura, N., et al. 2014, *Astrophys. J.* **789**, L39
- Watson, D., Hansen, C. J., Selsing, J., et al. 2019, *Nature* **574**, 497
- Webbink, R. F. 1984, *Astrophys. J.* **277**, 355
- Wehmeyer, B., Pignatari, M., Thielemann, F.-K. 2015, *MNRAS* **452**, 1970
- Wiescher, M., Görres, J., Thielemann, F.-K., Ritter, H. 1986, *Astron. & Astrophys.* **160**, 56
- Winteler, C., Käppeler, R., Perego, A., et al. 2012, *Astrophys. J.* **750**, L22
- Woosley, S. E., Taam, R. E., Weaver, T. A. 1986, *Astrophys. J.* **301**, 601
- Woosley, S. E., Weaver, T. A. 1986, *Lecture Notes in Physics* **255**, 91
- Woosley, S. E., Wilson, J. R., Mathews, G. J., Hoffman, R. D., Meyer, B. S. 1994, *Astrophys. J.* **433**, 229
- Wu, M.-R., Fischer, T., Huther, L., Martínez-Pinedo, G., Qian, Y.-Z. 2014, *Phys. Rev. D* **89**, 061303(R)
- Wu, M.-R., Fernández, R., Martínez-Pinedo, G., Metzger, B. D. 2016, *MNRAS* **463**, 2323
- Wu, M.-R., Barnes, J., Martínez-Pinedo, G., Metzger, B. D. 2019, *Phys. Rev. Lett.* **122**, 062701
- Zhu, Y. et al. 2018, *Astrophys. J.* **863**, L23
- Zingale, M. et al. 2018, *J. of Physics: Conference Series* **1031**, 012024